Go Green: General Regularized Green's Functions for Elasticity

Jiong Chen, Mathieu Desbrun

Go Green: General Regularized Green's Functions for Elasticity

JIONG CHEN, LTCI, Telecom Paris, Institut Polytechnique de Paris, France
MATHIEU DESBRUN, Inria / Ecole Polytechnique, France

The fundamental solutions (Green's functions) of linear elasticity for an infinite and isotropic media are ubiquitous in interactive graphics applications that cannot afford the computational costs of volumetric meshing and finite-element simulation. For instance, the recent work of de Goes and James [2017] leveraged these Green's functions to formulate sculpting tools capturing in real-time broad and physically-plausible deformations more intuitively and realistically than traditional editing brushes. In this paper, we extend this family of Green's functions by exploiting the anisotropic behavior of general linear elastic materials, where the relationship between stress and strain in the material depends on its orientation. While this more general framework prevents the existence of analytical expressions for its fundamental solutions, we show that a finite sum of spherical harmonics can be used to decompose a Green's function, which can be further factorized into directional, radial, and material-dependent terms. From such a decoupling, we show how to numerically derive sculpting brushes to generate anisotropic deformation and finely control their falloff profiles in real-time.

CCS Concepts: • **Computing methodologies** → **Volumetric models**.

Additional Key Words and Phrases: Green's functions, elasticity, anisotropic material, regularization, spherical harmonics.

ACM Reference Format:
Jiong Chen and Mathieu Desbrun. 2022. *Go Green:* General Regularized Green's Functions for Elasticity. In *Special Interest Group on Computer Graphics and Interactive Techniques Conference Proceedings (SIGGRAPH '22 Conference Proceedings), August 7–11, 2022, Vancouver, BC, Canada.* ACM, New York, NY, USA, 8 pages. https://doi.org/10.1145/3528233.3530726

1 INTRODUCTION

The fundamental solutions, or Green's functions, of anisotropic elasticity corresponding to point loads applied to an infinite elastic space are key in solid mechanics: their integral and Fourier-based expressions [Mura and Kinoshita 1972; Barnett 1972] have found applications in inclusion, dislocation, and crack problems [Xie et al. 2016]. In graphics, Green's functions have often been used to avoid the computational overhead involved in solving the elasticity equation when evaluating a static deformation under an imposed load, whether in animation [James and Pai 1999, 2003], shape editing [Lipman et al. 2008], or even water wave simulation [Schreck et al. 2019] and acoustics [James et al. 2006] to name a few applications. In the context of volume sculpting, this idea culminated recently with the Kelvinlets work of de Goes and James [2017, 2018]: they proposed real-time brushes for common modeling primitives such as grab, scale, twist, and pinch, based on a regularized version of these Green's functions which are free of computationally intensive solve and large memory requirement.

SIGGRAPH '22 Conference Proceedings, August 7–11, 2022, Vancouver, BC, Canada

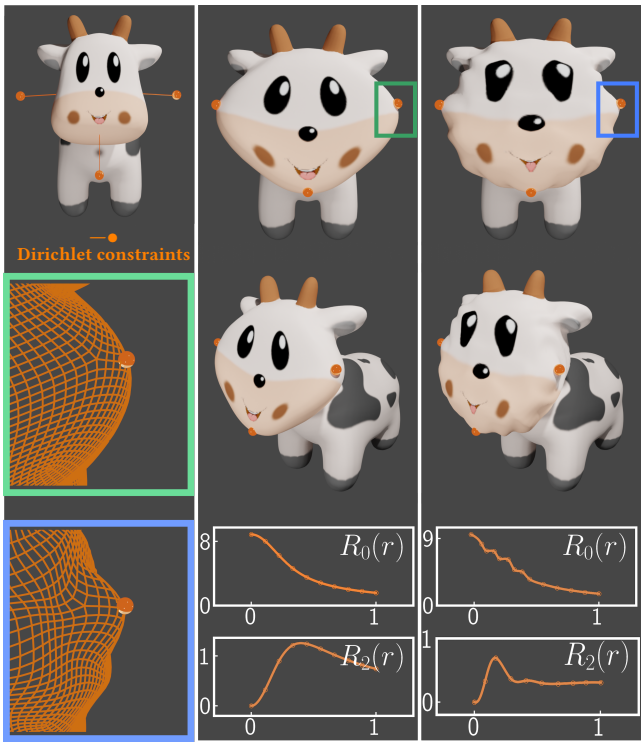

Fig. 1. **Meshes Go Green.** Our generalized Green's functions provide a variety of physically-based sculpting primitives offering fine artistic control over their spatial deformation in real-time. Here, the Spot model (top left) is deformed through an elastic displacement fitting prescribed constraints (middle); further manipulating the spline curves defining the radial decay of the deformation (bottom) allows for intuitive editing of the shape (right).

However, Kelvinlets are restricted to *isotropic* elastic objects, for which Green's functions have closed-form expressions. This severely constrains the look and feel of the brush-like deformations that can be rapidly evaluated on the fly during an editing session by a digital artist. Moreover, only limited control over the type of regularization of the inherently singular nature of Kelvinlets has been proposed [Cortez et al. 2005], which was partially remedied in recent extensions [de Goes and James 2019]. In this paper, we palliate these two limitations by offering *a fully general parameterization of the regularized Green's function of anisotropic elasticity.* In particular,

- we introduce a spherical harmonic (SH) expansion of Green's functions to represent the most general form of anisotropic linear elasticity, reproducing and extending the isotropic case of Kelvinlets without computational overhead; we also identify a decomposition of this expansion providing an intuitive use of these Green's functions for real-time volume sculpting.
- we present a general approach to regularize Green's functions by editing directly the radial integrals in the harmonic expansion

to offer intuitive artistic control over the falloff profile of the deformation generated by sculpting brushes.

2 REGULARIZED GREEN'S FUNCTIONS

In this section, we derive concrete expressions of regularized Green's functions for the anisotropic linear elasticity operator, which we will leverage later in Sec. 3 for the efficient implementation of sculpting tools. Since the loss of isotropy prevents the existence of simple closed-form solutions, we propose the use of spherical harmonics (SH) to offer a general expression of these Green's functions. Moreover, we identify a decomposition of this SH expansion into three decoupled terms: a directional term dealing with the anisotropic behavior, a radial term related to the regularized load which controls the propagation of a deformation away from the applied load, and a matrix term solely determined by the material itself. This decomposition is shown to offer simple and intuitive control over the physically-based deformation of arbitrary materials.

Notations. In the remainder of this paper, we use a **bold font** to denote vectors, matrices and high-order tensors, while an *italic font* is used for scalars. A wide $\widehat{\text{hat}}$ denotes the Fourier transform. Applied to vectors, |brackets| denote their lengths, while a $\widetilde{\text{tilde}}$ indicates their normalizations, i.e., a vector $\mathbf{v}$ is written $\mathbf{v} = |\mathbf{v}|\,\widetilde{\mathbf{v}}$.

2.1 General regularized Green's function

Definition. Given an external load $\mathbf{f}(\mathbf{x})$, the deformation (i.e., displacement) $\mathbf{u}\colon \mathbb{R}^3 \to \mathbb{R}^3$ of a linear elastic object is described (using Einstein's notation for repeated indices) through

$$C_{ijkl}\frac{\partial^2 u_k}{\partial x_l \partial x_j} + f_i = 0, \tag{1}$$

where $\mathbf{C} = [C_{ijkl}]$ is the fourth-rank elasticity tensor of the elastic material. Due to symmetries, this tensor has 21 independent components in the general case, but only two (the Lamé coefficients) when the material is isotropic [Kharevych et al. 2009]. Its regularized Green's function $\mathbf{G} : \mathbb{R}^3 \to \mathbb{R}^{3\times 3}$ is thus, by definition, satisfying:

$$C_{ijkl}\frac{\partial^2 G_{km}}{\partial x_l \partial x_j} + \delta_{im} g_\varepsilon(\mathbf{x}) = 0, \tag{2}$$

where G_{km} denotes the components of the tensor-valued function

$$\mathbf{G} = \begin{bmatrix} G_{11} & G_{12} & G_{13} \\ G_{21} & G_{22} & G_{23} \\ G_{31} & G_{32} & G_{33} \end{bmatrix},$$

δ_{im} is the Kronecker delta, and $g_\varepsilon(\mathbf{x})$ is a regularization of the Dirac delta distribution used in classical Green's functions. This smoothed load $g_\varepsilon(\mathbf{x})$ is typically assumed to be an arbitrary radially-symmetric function, parameterized by the width ε of its spatial support.

Explicit expression of Green's functions. To find a solution to Eq. (2), we first notice that the Fourier transform of G_{km} must satisfy:

$$\widehat{G}_{km}(\boldsymbol{\xi}) = (C_{ijkl}\xi_l\xi_j)^{-1}\delta_{im}\widehat{g}_\varepsilon(\boldsymbol{\xi}). \tag{3}$$

Applying the inverse Fourier transform [Barnett 1972] then yields:

$$\mathbf{G}(\mathbf{x}) = \frac{1}{8\pi^3}\int_{\mathbb{R}^3} \widehat{\mathbf{G}}(\boldsymbol{\xi})\exp(\mathbb{i}\,\mathbf{x}\cdot\boldsymbol{\xi})\,\mathrm{d}\boldsymbol{\xi}, \tag{4}$$

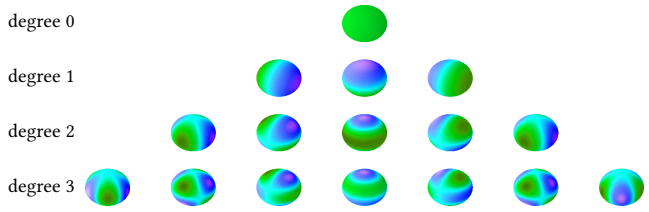

Fig. 2. **Real parts of spherical harmonics.** Spherical harmonics form a complete set of orthogonal basis functions which are particularly convenient to express spatial functions that are direction-dependent.

where $\mathbb{i}$ is the complex number satisfying $\mathbb{i}^2 = -1$, $\boldsymbol{\xi} \in \mathbb{R}^3$ is a phase vector in the spectral domain, while $\widehat{g}_\varepsilon$ is the Fourier transform of g_ε. Note that for a radial function g_ε, its Fourier transform $\widehat{g}_\varepsilon$ is also provably radial, and can be computed via the Hankel transform in 3D [Grafakos 2008, Appendix B.5]:

$$\widehat{g}_\varepsilon(\boldsymbol{\xi}) = \widehat{g}_\varepsilon(|\boldsymbol{\xi}|) = \frac{(2\pi)^{\frac{3}{2}}}{\sqrt{|\boldsymbol{\xi}|}}\int_0^\infty J_{\frac{1}{2}}(|\mathbf{x}||\boldsymbol{\xi}|)g_\varepsilon(|\mathbf{x}|)|\mathbf{x}|^{\frac{3}{2}}\,\mathrm{d}|\mathbf{x}|, \tag{5}$$

where J_α is the Bessel function of order α. As we review at length in the supplemental material (Sec. B), the Green's function for $\varepsilon = 0$ (i.e., with no regularization, corresponding to an impulse load) is singular at the origin — but a well-chosen smooth distribution g_ε can suppress this singularity. Once a regularized Green's function is obtained, the displacement field for a load $\mathbf{f}(\mathbf{x}) = g_\varepsilon(\mathbf{x}–\mathbf{x}')\,\mathbf{h}$ centered around $\mathbf{x}'$ (where $\mathbf{h}$ is a constant vector) becomes:

$$\mathbf{u}(\mathbf{x}) = \mathrm{Re}[\mathbf{G}(\mathbf{x}-\mathbf{x}')]\,\mathbf{h}, \tag{6}$$

where $\mathrm{Re}[\cdot]$ keeps only the real parts of its operand's components.

2.2 Spherical harmonic expansion

Given an arbitrary, non-degenerate $3\times3\times3\times3$ elasticity tensor $\mathbf{C}$, the integral in Eq. (4) may not have a closed-form expression. However, the plane-wave expansion, expressing a plane wave as a linear combination of spherical waves [Newton 2002] via:

$$\exp(\mathbb{i}\,\mathbf{x}\cdot\boldsymbol{\xi}) = 4\pi\sum_{l=0}^{\infty}\sum_{m=-l}^{l}\mathbb{i}^l j_l(|\mathbf{x}||\boldsymbol{\xi}|)Y_l^m(\widetilde{\mathbf{x}})\overline{Y}_l^m(\widetilde{\boldsymbol{\xi}}), \tag{7}$$

can be used to expand the Green's function $\mathbf{G}(\mathbf{x})$ into a spherical harmonic series, yielding:

$$\mathbf{G}(\mathbf{x}) = \frac{1}{2\pi^2}\sum_{l=0}^{\infty}\sum_{m=-l}^{l}\int_{\mathbb{R}^3}\widehat{\mathbf{G}}(\boldsymbol{\xi})\mathbb{i}^l j_l(|\mathbf{x}||\boldsymbol{\xi}|)Y_l^m(\widetilde{\mathbf{x}})\overline{Y}_l^m(\widetilde{\boldsymbol{\xi}})\,\mathrm{d}\boldsymbol{\xi}, \tag{8}$$

where $j_l(\cdot)$ is the spherical Bessel function, Y_l^m is the spherical harmonic function of degree l and order m, while $\overline{Y}_l^m$ is its complex conjugate, the latter two being evaluated at the normalized vectors $\widetilde{\mathbf{x}} = \mathbf{x}/|\mathbf{x}|$ and $\widetilde{\boldsymbol{\xi}} = \boldsymbol{\xi}/|\boldsymbol{\xi}|$ respectively.

Convenient decomposition. Since $\widehat{g}_\varepsilon$ is a radial function, Eq. (3) implies that the Green's function $\mathbf{G}$ can be rewritten as the sum over all degrees of spherical harmonics of a *product* of three parts:

$$\mathbf{G}(\mathbf{x}) = \frac{1}{2\pi^2}\sum_{l=0}^{\infty}\sum_{m=-l}^{l}\mathbb{i}^l\,Y_l^m(\widetilde{\mathbf{x}})\int_0^\infty \widehat{g}_\varepsilon(|\boldsymbol{\xi}|)j_l(|\mathbf{x}||\boldsymbol{\xi}|)\,\mathrm{d}|\boldsymbol{\xi}|\cdot \int_{\mathbb{S}^2}(C_{ikjl}\widetilde{\xi}_k\widetilde{\xi}_l)^{-1}\overline{Y}_l^m(\widetilde{\boldsymbol{\xi}})\,\mathrm{d}\mathbb{S}(\widetilde{\boldsymbol{\xi}}), \tag{9}$$

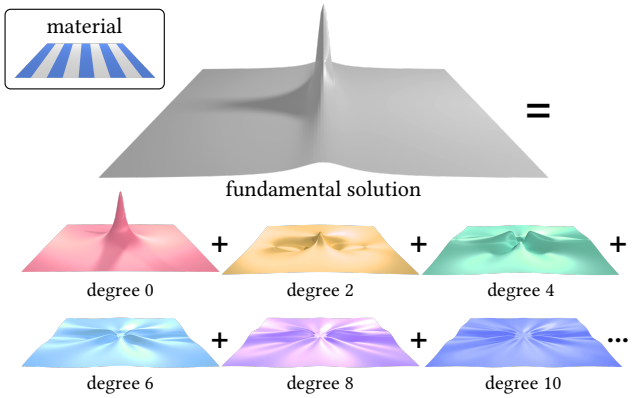

Fig. 3. **Spherical harmonic decomposition.** A flat composite made out of two materials (left inset, blue being stiffer than white) exhibits significant anisotropy: it stretches much more along the material stripes. For the equivalent homogenized anisotropic material, the Green's function for a regularized load (top) demonstrates this anisotropy, and it is well approximated using a weighted sum of low, even degrees of spherical harmonics.

where $\mathbb{S}^2$ is the unit sphere. This expression makes explicit the components of a Green's function of an arbitrary elasticity tensor onto the orthonormal basis of spherical harmonics. Rewriting Eq. (9) in spherical coordinates ($r \in \mathbb{R}^+, \theta \in [0,\pi], \varphi \in [0, 2\pi]$) yields the more concise expression:

$$\mathbf{G}(r,\theta,\varphi) = \frac{1}{2\pi^2} \sum_{l=0}^{\infty} \sum_{m=-l}^{l} \mathbb{i}^l \, Y_l^m(\theta,\varphi) \, R_l(r) \, \mathbf{P}_l^m(\mathbf{C}), \qquad (10)$$

where each $\mathbf{P}_l^m$, non-vanishing only for even degrees l, is a constant 3×3 matrix of imaginary values depending *only* on the elasticity tensor of the elastic material, while each R_l is a scalar radial function (we color-coded each term to make the connection with Eq. (9) obvious). This expression makes clear that the radial behavior of a Green's function around the load is explicitly related to the applied regularized load: when the Dirac delta function $g_0 = \delta$ is used, the integral of j_l leads to a singular function R_l at the origin (see Sec. B of the supplemental material); instead, a regularized $g_\varepsilon(\mathbf{x})$, integrated against the spherical Bessel functions removes the resulting singularity. To use this three-term expression, we will see in Sec. 3.1 that one can simply truncate this infinite sum to a given maximum degree $l_{\max}$.

2.3 Extension to affine loads

Similar to [Ainley et al. 2008; de Goes and James 2017], our SH-based regularized Green's functions can be extended to affine loads. When a regularized affine load of the form $\mathbf{F}(\mathbf{x}) = g_\varepsilon(\mathbf{x} - \mathbf{x}')\,\mathbf{H}$ (where $\mathbf{H}$ is a constant 3×3 matrix) is applied at a location $\mathbf{x}'$, the displacement field is assembled based on the gradient of the Green's function as:

$$\mathbf{u}(\mathbf{x}) = \mathrm{Re}\big[\nabla \mathbf{G}(\mathbf{x} - \mathbf{x}')\big] : \mathbf{H}, \qquad (11)$$

where $\nabla\mathbf{G}$ is a third-rank tensor, whose real part contracted with matrix $\mathbf{H}$ produces a displacement vector. As described in [de Goes and James 2017], affine loads allow for a variety of modeling primitives depending on the type of the matrix $\mathbf{H}$; for instance, scaling

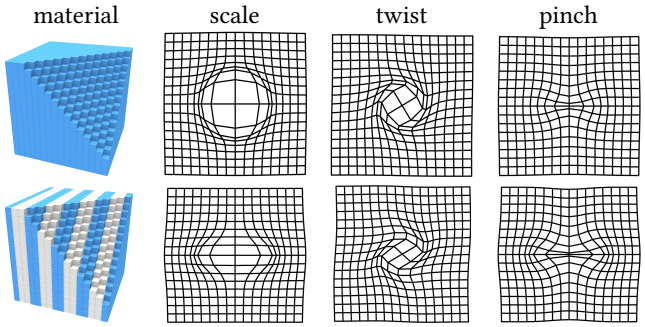

Fig. 4. **Deformation via affine loads.** The gradient of our Green's function allows the design of real-time sculpting brushes for common modeling primitives such as scale, twist, and pinch. While Kelvinlets can handle isotropic material (top), more complex anisotropic deformation can be obtained with our general Green's functions in the case of homogenized non-isotropic materials (bottom).

for a matrix proportional to the identity matrix, twisting for a skew-symmetric matrix, and pinching for a traceless matrix as depicted in Fig. 4. Noting that the partial derivative ∇_p with respect to spatial coordinate x_p simply amounts to a multiplication in the spectral domain, i.e.,

$$\widehat{G_{ij,p}} = \mathbb{i}\,\xi_p\,\widehat{G}_{ij}, \quad p = 0, 1, 2,$$

the partial derivative of $\mathbf{G}$ can also be re-expressed into three terms just like in Eq. (9), leading to a 3×3 matrix for each partial derivative $\nabla_p\mathbf{G}$ expressed as (we keep the color-coding convention for the three terms as used above):

$$\nabla_p \mathbf{G}(\mathbf{x}) = \frac{1}{2\pi^2} \sum_{l=0}^{\infty} \sum_{m=-l}^{l} \mathbb{i}^{l+1} \, Y_l^m(\widetilde{\mathbf{x}}) \, \mathcal{R}_l(|\mathbf{x}|) \, \boldsymbol{\mathcal{P}}_{l,p}^m(\mathbf{C}), \qquad (12)$$

where the two terms $\mathcal{R}_l$ and $\boldsymbol{\mathcal{P}}_{l,p}^m$ are expressed as:

$$\mathcal{R}_l(|\mathbf{x}|) = \int_0^\infty \widehat{g}_\varepsilon(|\xi|)\, j_l(|\mathbf{x}||\xi|)|\xi| \, \mathrm{d}|\xi|,$$

$$\boldsymbol{\mathcal{P}}_{l,p}^m(\mathbf{C}) = \int_{\mathbb{S}^2} (C_{ikjl}\widetilde{\xi}_k\widetilde{\xi}_l)^{-1} \overline{Y}_l^m(\widetilde{\boldsymbol{\xi}})\,\widetilde{\xi}_p \, \mathrm{d}\mathbb{S}(\widetilde{\boldsymbol{\xi}}).$$

In this affine load case, the material-dependent matrices $\boldsymbol{\mathcal{P}}_{l,p}^m$ are only non-vanishing for odd degrees ($l = 1, 3, 5\ldots$).

2.4 Controllable regularization

From Eq. (9), we observe that the only term involving the regularized load g_ε can be evaluated for any choice of regularization that leads to a *finite* integral. This allows us to choose the form of regularization to employ, and thus, to control the shape of the displacement away from the applied location. A canonical choice is, for instance, the normalized Gaussian distribution $g_\varepsilon(|\mathbf{x}|) = 1/(\varepsilon^3\pi^{3/2})\exp(-|\mathbf{x}|^2/\varepsilon^2)$, whose Fourier transform is $\widehat{g}_\varepsilon(|\xi|) = \exp(-\varepsilon^2|\xi|^2/4)$, yielding [Wolfram Research, Inc. 2021]:

$$\begin{aligned} R_l(r) &= \frac{\sqrt{\pi}}{2}\, r^l\, \varepsilon^{-l-1}\, \Gamma\left(\frac{l+1}{2}\right)\, {}_1\widetilde{F}_1\left(\frac{l+1}{2}; l+\frac{3}{2}; -\frac{r^2}{\varepsilon^2}\right), \text{ and} \\ \mathcal{R}_l(r) &= \sqrt{\pi}\, r^l\, \varepsilon^{-l-2}\, \Gamma\left(\frac{l}{2}+1\right)\, {}_1\widetilde{F}_1\left(\frac{l}{2}+1; l+\frac{3}{2}; -\frac{r^2}{\varepsilon^2}\right), \end{aligned} \qquad (13)$$

where Γ is the Gamma function and ${}_1\widetilde{F}_1$ is the regularized hypergeometric function. Fig. 5 shows these radial functions for the seven leading spherical harmonic degrees to demonstrate that the variance ε controls the radius of influence of the deformation.

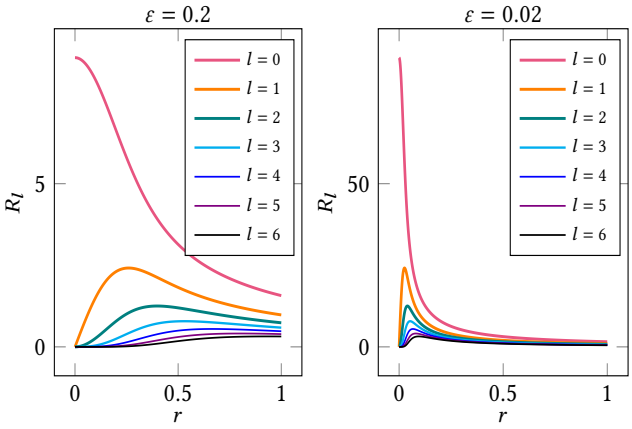

Fig. 5. **Gaussian-regularized $R_l(r)$.** Regularizing the Dirac delta impulse load ensures a finite Green's function at the origin; e.g., a normalized Gaussian load leads to a simple analytical expression for all radial functions R_l given in Sec. 2.4, where the radial decay of the fundamental solution is easily controlled by the Gaussian standard deviation ε, as shown for two different values above.

Implicit regularized load. While the regularization we just discussed or the one advocated in [de Goes and James 2017] suffices for many tasks, one may want a finer control over the radial decay of the elastic deformation around the applied location of the load since offering a choice in regularized loads is an important feature for modeling. Seemingly, deriving custom-made regularizations of the load raises a theoretical roadblock: constructing a large class of analytical functions g_ε that *ensure* the existence (finiteness) of the radial integral at the origin is not trivial. Fortunately, with our decomposition of Green's functions via spherical harmonics, we can *directly* edit the integrated radial function $R_l(|\mathbf{x}|)$ for each degree in order to customize a specific form of deformation attenuation around the point where the load is applied, and the shape of the edited curves intuitively maps to the resulting deformations, see Figs. 6 and 7 — we use cubic splines in our implementation as we will describe in Sec. 3.2 to offer easy and intuitive control to the artists. Choosing these functions R_l directly *defines* a regularized Green's function, whose actual mathematical expression could be extremely complex. It can be understood as an indirect regularization of the load; the regularized loads corresponding to prescribed radial functions may not even be continuous, but our approach bypasses a choice of a functional space for regularized loads that would unnecessarily limit the user's creativity: the final deformation is what visually matters.

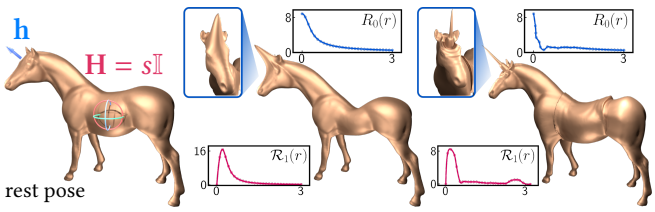

Fig. 6. **User-controlled falloff profiles.** Reshaping the radial functions $R_l(r)$ (resp., $\mathcal{R}_l(r)$) provides real-time artistic control over the elastic deformation generated by a load $\mathbf{h}$ (resp, affine load $\mathbf{H}$): it implicitly selects a regularization of the impulse load. Gaussian-regularized loads lead to smooth deformations of controllable radius (middle) of the rest pose (left); spline editing of the radial functions (right) affects the resulting deformation in a very intuitive manner as the closeups illustrate: note the effects of the small oscillations in the R_0 function on the horn-like deformation, and the saddle-like displacement due to the last bump in function $\mathcal{R}_1$.

2.5 Constrained deformation

Just like in the isotropic case, constraining a deformation pointwise can be achieved using Green's functions by solving a dense linear system. Given k points $\{\mathbf{x}_i\}_{i=0}^{k-1}$ and their prescribed displacements $\{\mathbf{u}_i\}_{i=0}^{k-1}$, a constrained deformation field can be found as the linear combination of k functions as $\mathbf{u}(\mathbf{x}) = \sum_i \mathrm{Re}[\mathbf{G}(\mathbf{x}-\mathbf{x}_i)]\,\mathbf{h}_i$, where the vectors $\{\mathbf{h}_i\}_{i=0}^{k-1}$ are solutions of the $3k \times 3k$ linear system:

$$\begin{bmatrix} \mathrm{Re}[\mathbf{G}(\mathbf{x}_0-\mathbf{x}_0)] & \dots & \mathrm{Re}[\mathbf{G}(\mathbf{x}_0-\mathbf{x}_{k-1})] \\ \vdots & \ddots & \vdots \\ \mathrm{Re}[\mathbf{G}(\mathbf{x}_{k-1}-\mathbf{x}_0)] & \dots & \mathrm{Re}[\mathbf{G}(\mathbf{x}_{k-1}-\mathbf{x}_{k-1})] \end{bmatrix} \begin{bmatrix} \mathbf{h}_0 \\ \vdots \\ \mathbf{h}_{k-1} \end{bmatrix} = \begin{bmatrix} \mathbf{u}_0 \\ \vdots \\ \mathbf{u}_{k-1} \end{bmatrix}.$$

Once the left hand side matrix is prefactorized, one can easily add a few more constraints interactively using low rank updates as explained in [de Goes and James 2017], see Fig. 1.

3 RESULTS

Equipped with the expressions of the general Green's functions and the various resulting deformation fields we derived, we can now focus on how to leverage them numerically to derive physically-plausible digital sculpting tools facilitating the real-time and intuitive editing of an arbitrary shape without requiring any expensive volumetric meshing or finite-element simulation.

3.1 Implementation details

The implementation of our Green's functions and associated displacements is rather straightforward as it relies on the evaluation of a truncated sum of terms that are either trivial to evaluate at runtime or simple to precompute offline. A C++ code is available at `https://gitlab.inria.fr/geomerix/public/gogreen`, where special functions such as spherical harmonics and hypergeometric functions are computed using the `boost` [Boost 2021] and `GSL` [Gough 2009] libraries. We discuss our choice of truncation next to ensure both efficiency and generality.

Analysis of the spherical harmonic expansion. Once the elasticity tensor $\mathbf{C}$ of an elastic material is given, one can directly evaluate a deformation field through Eq. (6) or Eq. (11). However, truncating the infinite sum of the Green's function may lead to numerical artifacts in general. To properly evaluate the effect of truncation, we compute the approximate deformation fields $\mathbf{u}^{[l_{\max}]}(\mathbf{x})$ for various elastic materials from Fig. 12 using a fixed load, computed from the Green's function in Eq. (10) where the sum is truncated after the first $l_{\max}$ degrees. We also estimate the exact deformation fields $\mathbf{u}$ to

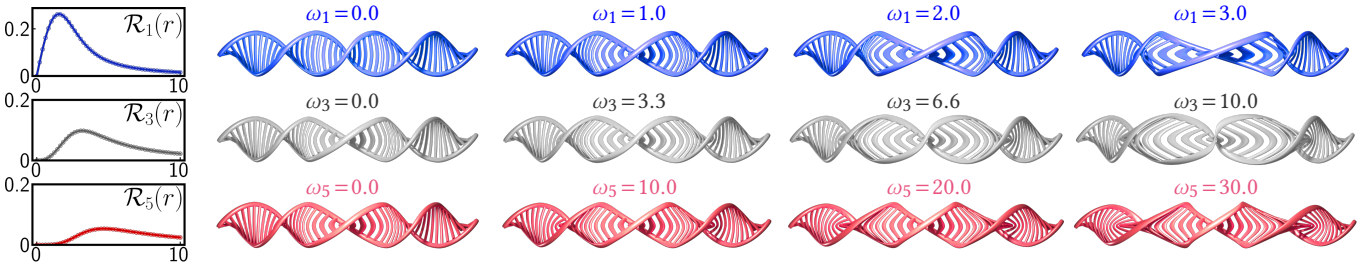

Fig. 7. **Pinch control.** In contrast to Kelvinlets, we have full control over the falloff profile of a deformation. For a DNA double helix pinched in the middle for instance, scaling one of the low-degree radial functions $\mathcal{R}_1, \mathcal{R}_3$ or $\mathcal{R}_5$ with $\omega_{i=1,3,5}$ respectively tunes the magnitude of the deformation from global to local. The user selected a LAYERED material (second choice in Fig. 12) for this example. Deriving physically-based deformation via volumetric meshing and simulation of this model would not be even close to interactive; our evaluation of anisotropic Green's functions is thus the only viable real-time editing tool here.

high accuracy using a high-order (5810-point) Lebedev quadrature, accurate to the 131st algebraic order, for the evaluation of the spherical integration in $\mathbf{P}_l^m(\mathbf{C})$ since no analytical solutions are known. We then deduce the relative error $\delta = \int_\Omega \|\mathbf{u}^{[l_{\max}]} - \mathbf{u}\| \, d\mathbf{x} / \int_\Omega \|\mathbf{u}\| \, d\mathbf{x}$. Fig. 9 shows that the elastic displacement is very well approximated using only a few spherical harmonic degrees; one can see that the approximation error decays fast with the max degree $l_{\max}$ for all the elasticity tensors, with the worst error happening for a material that is extremely anisotropic in one single direction — which is expected as the decay rate of the spherical harmonic coefficients depends mostly on spatial smoothness. When the relative truncation error is below 10^{-2}, results are visually indistinguishable from the exact solution. In order to handle accurately and efficiently most anisotropic materials, we thus truncate the sum at $l_{\max} = 8$ in practice, resorting to $l_{\max} = 20$ *only* for extremely strong anisotropy. Note finally that no discontinuity is created by our truncation, since all terms are spatially smooth.

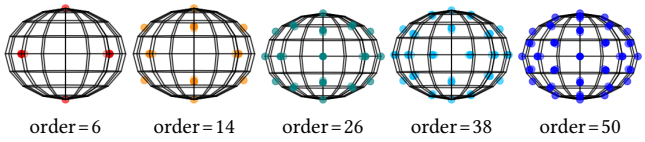

Fig. 8. **Lebedev quadrature points.** As the number of evaluation points grows, Lebedev quadrature offers an approximation to the surface integral of any function over the unit sphere up to a certain order of accuracy, exactly capturing the integral of spherical harmonics of increasing degrees.

Fast evaluation of elastic displacements. In the truncated summation of the Green's functions in Eq. (10) (resp., of its gradient in Eq. (12)), the matrix-valued terms $\mathbf{P}_l^m$ (resp., $\boldsymbol{\mathcal{P}}_{l,p}^m$) are only non-vanishing for even degrees $l = 0, 2, 4\ldots$ (resp., odd degrees $l = 1, 3, 5\ldots$), so one can safely ignore half of the degrees for efficiency. Similarly, for each degree l, the real parts for m and $-m$ ($m \leq l$) are equal, further decreasing the evaluation cost by half. When the material is purely isotropic, its evaluation further reduces to only non-zero values for degrees 0 and 2 (resp., for degrees 1 and 3): in this case, the expression of Eq. (9) is exactly the Kelvin solution when $g_\varepsilon(\mathbf{x}) = \delta(\mathbf{x})$, and the regularized Kelvin solution [Cortez et al. 2005; de Goes and James 2017] when $g_\varepsilon(\mathbf{x}) = 15\varepsilon^4/(8\pi)(|\mathbf{x}|^2 + \varepsilon^2)^{-7/2}$ as we prove in the supplemental material (Sec. B). For a material with a general anisotropic elasticity tensor $\mathbf{C}$, one may wonder if there are simple closed-form expressions for all degrees l. We sidestep this issue by applying a discrete quadrature rule to evaluate the matrices $\mathbf{P}_l^m$ and $\boldsymbol{\mathcal{P}}_{l,p}^m$ numerically in a *preprocessing step*: we simply precompute numerical approximations of their integral expressions up to degree $l_{\max}$. We rely on *Lebedev quadrature* in our implementation, systematically using the Lebedev quadrature locations and weights from [Burkardt 2020] with an accuracy order of 194 by default, see Fig. 8. We thus obtain a fast, on-the-fly evaluation of the displacement field given in Eq. (6) or Eq. (11) at runtime using these precomputed matrices $\mathbf{P}_l^m$ and $\boldsymbol{\mathcal{P}}_{l,p}^m$ since the spherical harmonics Y_l^m are computed analytically and the radial functions R_l and $\mathcal{R}_l$ are either known analytically for simple choices of regularization or through spline evaluation otherwise as we will describe in Sec. 3.2. While our implementation relies on CPU evaluation, implementing our approach on the GPU as a geometry shader would lead to faster running times, since massively-parallel processing of all the mesh nodes of a model is simple due to our expressions requiring only a few precomputed terms.

3.2 Real-time volume sculpting

Our fast evaluation of generalized Green's functions and their associated displacements are particularly amenable to real-time volume sculpting: as demonstrated in [de Goes and James 2017], a number of modeling operations can be derived from the fundamental solution of elasticity to capture broad volume deformations. They result

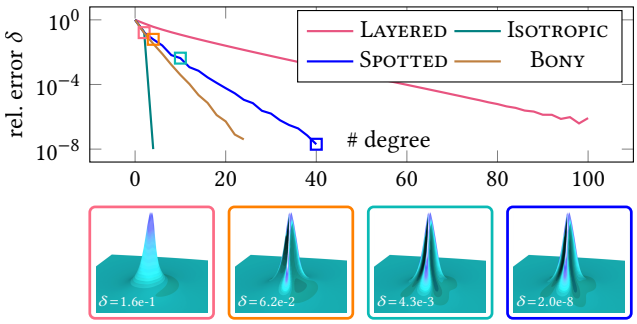

Fig. 9. **Error dependence on SH degrees.** For the bimaterials from Fig. 12 with a contrast of 10^2, we measure the L_2 relative error δ of a deformation field as a function of the number of spherical harmonic degrees used in its evaluation (top). For the spotted material, truncating after only eight degrees is already visually indistinguishable from the exact solution as evidenced by the mean-curvature plots for truncations after 0, 2, 8 and 38 degrees.

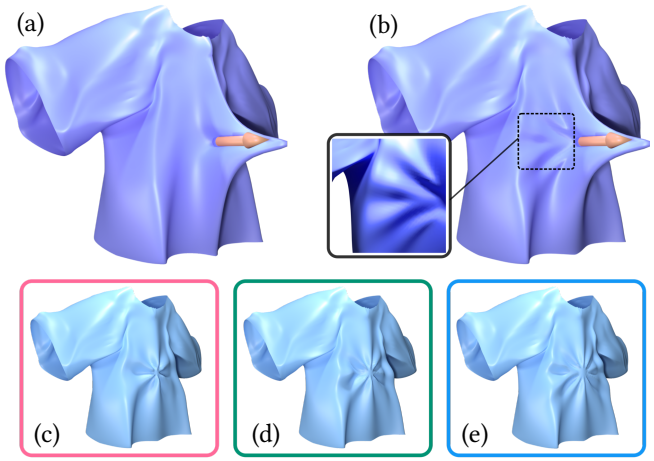

Fig. 10. **Wrinkle design.** Strong material anisotropy generates wrinkle-like components of various fold counts ($l = 6, 8, 10$ for (c), (d) and (e)) when projected onto spherical harmonics. One can thus turn a regular grab (a) into a wrinkle brush (b) through either early truncation, or by reweighting these physically plausible components.

in more intuitive and realistic effects than traditional Maya-like brushes that often fail to offer physically-plausible editing. All the digital modeling tools using their regularized Kelvinlets (brushes, compound brushes, gradient contraints, symmetrized deformations) can be straightforwardly adapted to our more general framework, where now anisotropy of the material is leveraged to offer a wider range of volume sculpting. In this section, we provide a series of examples showcasing the intutive nature and visual quality of our physically-based deformation tools compared to existing sculpting tools; in particular, we show how the multiscale extrapolation proposed in the original Kelvinlets paper finds a simpler, more flexible solution through our expansion decomposition and its radial term.

User interface. Our overall approach to digital sculpting closely follows the work of de Goes and James [2017]: a selection of brushes is offered to the user, and once selected, the brush center is assigned to the mouse click location. By default, we use a Gaussian-regularized Green's function for an isotropic material, parameterized with the radius of influence ε and the Lamé coefficients over which the user has interactive control. During a mouse event, we deform all the vertices within a ball around the brush by moving them along the streamlines defined by the elastic displacement field to ensure a physically-plausible deformation.

Anisotropy control. The user selects the deformation behavior she seeks by providing a particular type of anisotropic elasticity. For simple cases such as transverse isotropy or orthotropy, the elasticity tensors are parameterized through simple and intuitive Young's moduli, shear moduli and Poisson ratios (see Sec. A in the supplemental material) — the user can thus specify each parameter to realize anisotropy control as demonstrated in Fig. 11. However, for more general anisotropic cases, directly prescribing an elastic tensor C through its 21 independent coefficients in Voigt form is no longer intuitive or even concise. We found quite convenient to prescribe

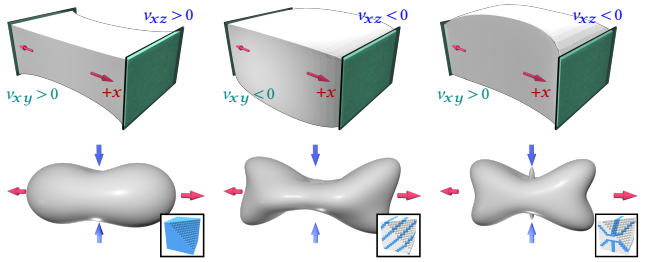

Fig. 11. **Anisotropic manipulation.** (top) Stretching an orthotropic cube along one direction causes shrinkage or inflation along the other directions depending on prescribed Poisson ratios. (bottom) Homogenizing composite materials (insets) provides rich gamut of physical behaviors even for a simple stretching and pinching of a sphere.

an arbitrary material by selecting one of a few proposed patterns of bimaterials (and a rotation, to align the anisotropy with a given direction) that we then homogenize to its equivalent anisotropic elastic tensor using the approach of [Kharevych et al. 2009]. The patterns are simply defined by assigning one of two isotropic materials for each cell of a 16×16×16 regular grid. The user has also interactive control over the stiffness contrast between the two isotropic materials. This simple interface offers intuitive control over the Green's functions by selecting the resulting symmetry of the material tensor via the spatial symmetry of its associated geometric patterns as shown in Fig. 12. The homogenized elastic tensor is represented as a symmetric 6×6 matrix $\mathbf{C}^V$, re-expressing the fourth-order tensor C_{ijkl} based on the Voigt notation for reduced storage. Fig. 11 shows the stretching of an orthotropic cube for various Poisson ratios, and a pinched & stretched sphere for three different materials: while pinching an isotropic material generates the expected bean-like shape, anisotropic materials generate richer deformations.

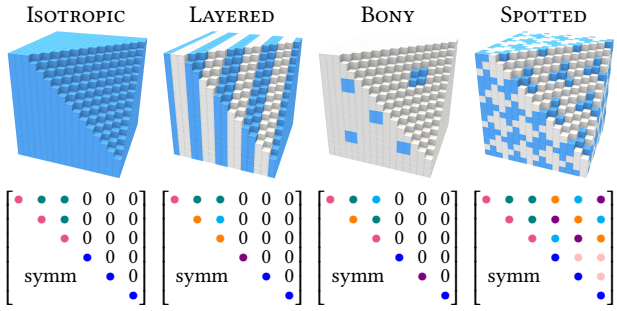

Fig. 12. **Material Homogenization.** Homogenized elasticity tensor of a few bimaterials, expressed in reduced Voigt notation [Kharevych et al. 2009], where for a given material, same-color coefficients indicate equal values, reflecting the symmetries of its elasticity tensor.

Regularization and falloff profile control. As we reviewed in Sec. 2.2, our three-term decomposition of a generalized Green's function provides a very convenient way to control the radial behavior of deformation fields: one can directly choose the radial function R_l or $\mathcal{R}_l$ for one or more spherical harmonic degrees. This property has important consequences for modeling purposes. A limitation of Kelvinlets for a canonical regularized load is its fixed spatial decay, which requires a special, multiscale extrapolation to construct

brushes with arbitrarily decays involving a linear combination of deformations; a recent extension [de Goes and James 2019] simplifies this construction, but still offers only limited control over spatial falloff. Instead, our radial functions offer a convenient, indirect way to choose a regularized load as argued in Sec. 2.4; but it also provides a *simple and straightforward* way to define falloff profiles that control the locality of deformation, more in line with traditional brushes [Angelidis et al. 2004]. As mentioned earlier, we assign our radial functions R_l (up to degree $l_{\max}$) by default to the Gaussian-regularized function from Eq. (13) parameterized by a scale ε. As Fig. 5 shows, R_0 is significantly larger than all the others, and it is also the only one not valued zero at the origin. We convert these functions into cubic splines by evaluating their analytical values on regular samples with a density based on the local mesh resolution of the model in order to control even its smallest scale. The user can then freely edit the curves to achieve her desired look: for instance, adding a few wiggles in R_0 by dragging its control points up and down adds bumps to a deformation as demonstrated in Fig. 1, while editing the second radial function R_2 further insert fine details. We found that only editing R_0 and R_2 (resp., $\mathcal{R}_1$ and $\mathcal{R}_3$ for gradient-based brushes) is enough to offer a very rich spectrum of deformations: the other radial basis functions are less visually impacting, and are thus less worth editing, see Fig. 7. Finally, we maintain the zero value of all $R_{l>1}$ at the origin so that the maximum magnitude of the deformation remains at the center of the modeling brush. Fig. 6 further shows how edits of the spline curves R_0 and $\mathcal{R}_1$ allow for fine artistic control.

Timing. We performed a number of tests on a desktop with a 32-core Intel® Xeon® Silver CPU. We found that evaluating the spherical harmonic series per point has a complexity in $O(l_{\max}^2)$ as shown in Fig. 13(a), and that the calculation of a displacement vector takes less than $0.015ms$ when $l_{\max} = 8$. In terms of scalability, processing time grows linearly in the number of points to displace (Fig. 13(b)), and the constant scaling of the complexity is mostly determined by the number of threads available for parallellization. In our tests, 10^6 points only require about $440ms$ for their displacement calculation using 56 threads and $l_{\max} = 8$. The massive parallellism provided by GPUs would undoubtedly lead to considerable speedups.

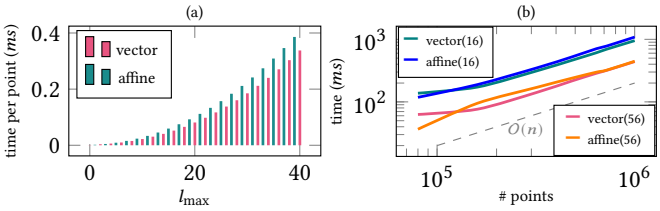

Fig. 13. **Timing.** For both vector and affine loads, we count: (a) per-point computational cost for a truncation of the SH series at $l_{\max}$; (b) total computational cost with respect to the number of points evaluated for $l_{\max} = 8$ using 16 and 56 threads respectively.

Exploiting Gibbs phenomenon for wrinkling. While toying with our modeling brushes, we also stumbled upon an unexpected side effect that we turned into a feature. We noticed that for very anisotropic materials, the fundamental solution of elasticity expressed as a weighted sum of spherical harmonics include interestingly complex individual terms, even if the total sum is rather simple: Fig. 4 shows that the solution of a regularized load applied on a strongly anisotropic material includes, for each SH degree, deformation fields that are more complex than the total deformation, akin to a form of Gibbs phenomenon. Truncating the Green's function at $l_{\max} = 4$ for instance thus maintains smoothness and physical plausibility of the deformation, but offers wrinkle-like features. Fig. 10 shows how such an early truncation or the use of selected degrees turns a regular grab brush into a wrinkling brush, where directionality is easily adjusted through rotation of the anisotropy of the material and of the associated SH-projected material coefficients [Green 2003].

4 CONCLUSIONS

In this paper, we have extended the family of deformation tools based on regularized fundamental solutions of linear elasticity proposed in [de Goes and James 2017] by considering anisotropic materials. Our expression of the fully-general Green's functions for the elasticity operator based on a spherical harmonic expansion was shown to factor into three terms, which we leveraged for efficient evaluation and intuitive control of physically-based deformation. Despite generalizing the original Kelvinlets approach to arbitrary homogeneous elastic materials, our method still provides real-time volume sculpting tools by avoiding volumetric discretization or elastic simulation of the model. It also provides far enhanced control over both the directionality and falloff profile of the editing tools, as well as a richer gamut of physically-derived spatial deformation. While we only exploited our general Green's functions and their numerical approximation for real-time sculpting, they may also apply to a number of other interactive applications.

Future work. While Green's functions for elasticity are traditionally describing the solutions for an infinite *homogeneous* material, it would be interesting to adapt our method to account for inhomogeneity. One could, for instance, use a spatial blending function to interpolate between local elasticity tensors in Eq. (2) and derive the associated Green's function via Fourier transform. Note that our approach could also be applied for elastic dynamics, where the Fourier transform of the associated Green's functions should be a solution to a second-order ODE in frequency domain; control over the propagation of elastic waves might ease the creation of animation. Moreover, imposing boundary conditions typically requires a dense linear system solve, which can become inefficient as the number of constraints grows — as is typical of the boundary element method. Analyzing the locality of our Green's functions as a function of their radial regularization and incorporating a fast multipole method could help reduce computational complexity. Finally, a statistical approach like Walk-on-Sphere [Sawhney and Crane 2020] might be well adapted to offer fast previews of the solutions to large-scale anisotropic equations with boundary conditions.

ACKNOWLEDGMENTS

The 3D models in this paper are courtesy of Keenan Crane (Fig. 1), AIM@SHAPE (Fig. 6), and ARCSim (Fig. 10). The authors would like to thank Fernando de Goes for inspiring discussions and feedback, and the reviewers for their constructive comments. The authors

acknowledge the generous support of a Choose France Inria chair, and of Ansys, Inc.

REFERENCES

Josephine Ainley, Sandra Durkin, Rafael Embid, Priya Boindala, and Ricardo Cortez. 2008. The method of images for regularized Stokeslets. *J. Comput. Phys.* 227, 9 (2008), 4600–4616.

Alexis Angelidis, Geoff Wyvill, and Marie-Paule Cani. 2004. Sweepers: swept user-defined tools for modeling by deformation. In *Proceedings of Shape Modeling Applications*. 63–73.

David M. Barnett. 1972. The precise evaluation of derivatives of the anisotropic elastic Green's functions. *Physica Status Solidi (b)* 49, 2 (1972), 741–748.

Boost. 2021. Boost C++ Libraries. http://www.boost.org/.

John Burkardt. 2020. Quadrature Rules for the Unit Sphere. https://people.sc.fsu.edu/~jburkardt/cpp_src/sphere_lebedev_rule/sphere_lebedev_rule.html

Ricardo Cortez, Lisa Fauci, and Alexei Medovikov. 2005. The method of regularized Stokeslets in three dimensions: analysis, validation, and application to helical swimming. *Physics of Fluids* 17, 3 (2005), 031504.

Fernando de Goes and Doug L James. 2017. Regularized Kelvinlets: sculpting brushes based on fundamental solutions of elasticity. *ACM Trans. Graph.* 36, 4 (2017), 1–11.

Fernando de Goes and Doug L James. 2018. Dynamic Kelvinlets: secondary motions based on fundamental solutions of elastodynamics. *ACM Trans. Graph.* 37, 4 (2018), 1–10.

Fernando de Goes and Doug L. James. 2019. Sharp Kelvinlets: Elastic Deformations with Cusps and Localized Falloffs. In *Digital Production Symposium*. Article 2.

Brian Gough. 2009. *GNU Scientific Library Reference Manual* (third ed.). Network Theory Ltd.

Loukas Grafakos. 2008. *Classical fourier analysis* (second ed.). Springer.

Robin Green. 2003. Spherical harmonic lighting: The gritty details. In *Archives of the game developers conference*, Vol. 56. 4.

Doug L James, Jernej Barbič, and Dinesh K Pai. 2006. Precomputed acoustic transfer: output-sensitive, accurate sound generation for geometrically complex vibration sources. *ACM Trans. Graph.* 25, 3 (2006), 987–995.

Doug L James and Dinesh K Pai. 1999. Artdefo: accurate real time deformable objects. In *Proceedings of the Conference on Computer Graphics and Interactive Techniques*. 65–72.

Doug L James and Dinesh K Pai. 2003. Multiresolution Green's function methods for interactive simulation of large-scale elastostatic objects. *ACM Trans. Graph.* 22, 1 (2003), 47–82.

Lily Kharevych, Patrick Mullen, Houman Owhadi, and Mathieu Desbrun. 2009. Numerical coarsening of inhomogeneous elastic materials. *ACM Trans. Graph.* 28, 3 (2009), 1–8.

Yaron Lipman, David Levin, and Daniel Cohen-Or. 2008. Green coordinates. *ACM Trans. Graph.* 27, 3 (2008), 1–10.

Toshio Mura and N Kinoshita. 1972. The precise evaluation of derivatives of the anisotropic elastic Green's functions. *Physica Status Solidi (b)* 49, 2 (1972), 741–748.

Roger G. Newton. 2002. *Scattering Theory of Waves and Particles*. Springer-Verlag.

Rohan Sawhney and Keenan Crane. 2020. Monte Carlo geometry processing: A grid-free approach to PDE-based methods on volumetric domains. *ACM Trans. Graph.* 39, 4 (2020).

Camille Schreck, Christian Hafner, and Chris Wojtan. 2019. Fundamental solutions for water wave animation. *ACM Trans. Graph.* 38, 4 (2019), 1–14.

Wolfram Research, Inc. 2021. Mathematica (version 13.0.0). https://www.wolfram.com/mathematica

Longtao Xie, Chuanzeng Zhang, Jan Sladek, and Vladimir Sladek. 2016. Unified analytical expressions of the three-dimensional fundamental solutions and their derivatives for linear elastic anisotropic materials. *Proceedings of the Royal Society A: Mathematical, Physical and Engineering Sciences* 472, 2186 (2016), 20150272.